Olsson, Anders; Tiira, Jonna; Partanen, Mikko; Hakkarainen, Teemu; Koivusalo, Eero; Tukiainen, Antti; Guina, Mircea; Oksanen, Jani

Optical energy transfer and loss mechanisms in coupled intracavity light emitters

Please cite the original version:
Olsson, A., Tiira, J., Partanen, M., Hakkarainen, T., Koivusalo, E., Tukiainen, A., ... Oksanen, J. (2016). Optical energy transfer and loss mechanisms in coupled intracavity light emitters. IEEE Transactions on Electron Devices, 63(9), 3567-3573. https://doi.org/10.1109/TED.2016.2590461

Optical energy transfer and loss mechanisms in coupled intracavity light emitters

Anders Olsson, Jonna Tiira, Mikko Partanen, Teemu Hakkarainen, Eero Koivusalo, Antti Tukiainen,
Mircea Guina, and Jani Oksanen

Abstract—**Despite the near-unity internal quantum efficiencies (IQEs) demonstrated for GaAs based light emitters, laser cooling of the ubiquitous III-V semiconductors has not been feasible. The key challenges for III-V optical cooling are the reduced absorption of the optical excitation at photon energies well below the band gap and the strong confinement of the light in the high refractive index semiconductors. Here we investigate the possibility to eliminate the need for light extraction and to eventually relax the requirements of the IQE. This is done by using electroluminescence and optical energy transfer within intracavity devices consisting of an AlGaAs/GaAs double heterojunction LED and a GaAs pn-homojunction photodiode enclosed within a single semiconductor cavity. We measure the intracavity energy transfer i.e. the coupling quantum efficiency (CQE) between the two diodes and estimate loss mechanisms by simultaneously measuring the IV-characteristics of the emitter diode and the photocurrent of the absorber diode. The measured CQE is below 60 % due to the mirror, light extraction, nonradiative and detection losses. While this is far below the state-of-the-art efficiencies, our results suggest that it will be possible to substantially improve the efficiency by adopting the fabrication and design principles used for the best performing photoluminescent emitters.**

Index Terms—**Light emitting diodes, photodiodes, semiconductor heterostructures, optical energy transfer**

I. INTRODUCTION

During the past few decades the research of planar optoelectronic devices has strongly focused on solving the scientific and technological challenges introduced by gallium nitride [1] and emerging nitride and antimonide based material systems [2] drawing attention away from conventional III-V semiconductors. Recent advances and increased awareness of the possibilities to harness the thermodynamics of light emission in new applications such as optical cooling [3], [4] together with optimization of light emission efficiency [5], [6] and information processing [7] have, however, started to reinforce the research interests in the mature III-V materials.

The progress of the solid state optical cooling technologies has been pioneered by the laser cooling of doped glasses [3], but also laser cooling of semiconductors [4] and very low power electroluminescent (EL) cooling of small band gap light-emitting diodes (LEDs) has recently been demonstrated

A. Olsson is with The Department of Micro- and Nanosciences, Micronova, Aalto University, P.O. Box 13500, FI-00076, Finland and with The Engineered Nanosystems Group, Aalto University, P.O. Box 12200, FI-00076, Finland.

J. Tiira, M. Partanen and J. Oksanen are with The Engineered Nanosystems Group, Aalto University, P.O. Box 12200, FI-00076, Finland.

T. Hakkarainen, E. Koivusalo, A. Tukiainen and M. Guina are with The Optoelectronics Research Centre, Tampere University of Technology, P.O. Box 692, FI-33101, Finland.

[8], [9]. Despite some efforts to harness optical tunneling over vacuum nanogaps to overcome the light extraction problem in typical cooling experiments [3], [10], the light confinement due to large refractive index of typical semiconductors has remained one of the largest obstacles in demonstrating optical cooling of semiconductors [11].

In this paper we investigate the effects of enclosing an LED and a light absorbing photodiode within the same semiconductor crystal in an intracavity configuration that allows straightforward electrical characterization and essentially eliminates the light extraction issues encountered in conventional setups. Unlike laser cooling, where the excitation power quickly drops when the photon energy of the excitation drops below the band gap energy, using an LED based approach also allows using bias voltages and excitation energies that are well below the threshold set by the band gap. Therefore the presently studied intracavity approach can substantially relax the material requirements for reaching the high current EL cooling regime and thereby eventually considerably facilitate observing EL cooling under high current conditions.

II. EXPERIMENT

A. Samples

The devices studied in this work each consist of a double heterojunction (DHJ) GaAs/AlGaAs LED structure grown on top of a GaAs p-n homojunction photodiode. The device schematic and basic device structure is shown in Fig 1. The light emitted by the DHJ LED is guided towards the GaAs photodiode either directly or after a single reflection from the top contact. Measuring the current of the photodiode allows a straightforward means to detect the absorbed light without the need to extract it from the high refractive index semiconductor material.

The fabrication of the four distinct epitaxial structures studied in this work was carried out by using molecular beam epitaxy (MBE). The key difference between these samples is the thickness of the GaAs active layer (AL) of the DHJ LED structure, which was 300 nm for epistructures A1 and B1 and 50 and 10 nm for structures B2 and B3, respectively. In sample A1 the GaAs homojunction of the photodiode additionally included an intrinsic GaAs-layer sandwiched between the p- and n-doped layers. The layer thicknesses and the doping concentrations of the structures are described in more detail in Table I.

Each epistructure was subsequently processed to contain a selection of circular mesas of different diameter and contact
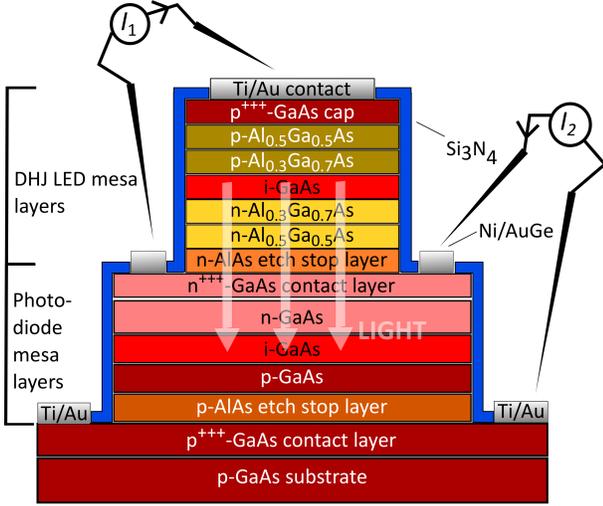
Figure 1. A schematic illustration of the DHJ structure and the coupling quantum efficiency measurement setup, where I_1 denotes the current driving the DHJ LED, and I_2 the current measured from the photodiode. The coupling quantum efficiency is defined as $\eta_{\mathrm{CQE}} = I_2/I_1$.

Table I
THE LAYER STRUCTURES USED IN THIS WORK WITH THE DIFFERENCES
BETWEEN THE STRUCTURES COMPARED TO STRUCTURE B1 BOLDED.

Material	Doping (cm^{-3})	Layer thickness (nm)			
		A1	B1	B2	B3
p-GaAs cap	1.0e19	20	20	20	20
p-Al$_{0.5}$Ga$_{0.5}$As	1.0e19	**100**	200	200	200
p-Al$_{0.3}$Ga$_{0.7}$As	3.0e17	**300**	500	500	500
i-GaAs	-	300	300	**50**	**10**
n-Al$_{0.3}$Ga$_{0.7}$As	1.3e17	300	300	300	300
n-Al$_{0.5}$Ga$_{0.5}$As	1.3e17	800	800	800	800
n-AlAs	1.0e18	5	5	5	5
n-GaAs	5.6e18	20	20	20	20
n-GaAs	1.0e18	700	700	700	700
i-GaAs	-	**1000**	0	0	0
p-GaAs	3.0e17	3000	3000	3000	3000
p-AlAs	3.0e18	15	15	15	15
p-GaAs	1.0e19	50	50	50	50
p-GaAs substrate	1.0e18				

regions providing electrical contacts to the LED and the photodiode, as detailed in Figures 1-2 and in Table II. To form the contacts, Ti/Au and Ni/AuGe layers with thicknesses 15/200 nm were deposited on top of the heavily doped p- and n-GaAs regions, respectively. In selected p-type contacts formed on top of the mesas, the contacts were additionally patterned, as illustrated in Fig. 2, so that a large fraction of the GaAs capping layer was replaced by a 360 nm thick Si$_3$N$_4$ layer to form an omnidirectional reflector (ODR) to increase the contact reflectance. The ODR fill factors and contact radii used to form the ODR contacts are listed in Table II. The mesas were fabricated using standard semiconductor processing techniques, in a process containing several repeated steps of UV-lithography, wet etching, contact metal evaporation and lift-off.
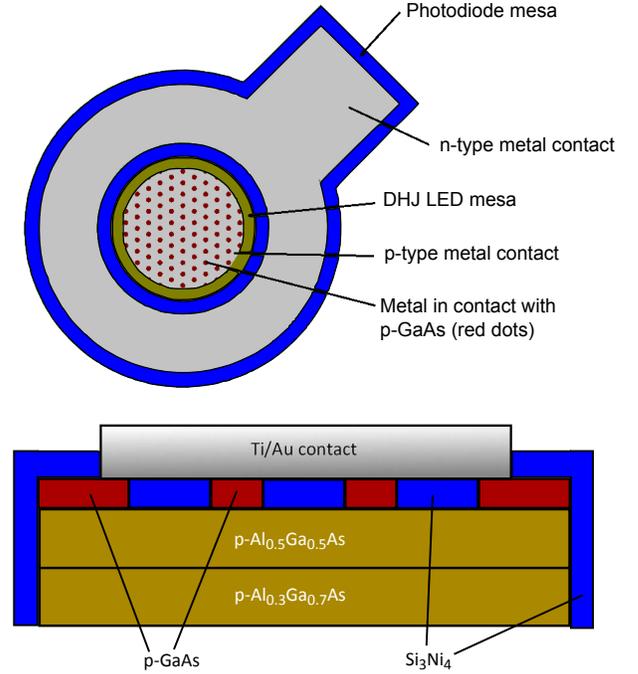

Figure 2. Top and side-view schematics of a mesa showing the partially etched p-GaAs cap layer and the Si$_3$Ni$_4$ ODR mirror used to prevent light absorption in the cap layer.

B. Measurements

The main characterization of the samples was done in a 4-point probe setup where the IV characteristics of the DHJ LED were measured while simultaneously measuring the IV characteristics of the lower diode, as illustrated in Fig. 1. As this IV-IV measurement provides direct information on both the electrical characteristics and optical emission of the LED, it provides an attractive and simple method to characterize the intracavity structures. Combining the IV-IV results obtained for a set of samples with different AL thickness and top contact designs to measurements while submerged in media with varying refractive indices we can not only measure the efficiency of energy transport between the diodes, but also qualitatively draw conclusions on the importance of the key loss mechanisms in the structures. These losses include mainly nonradiative recombination, optical transport (absorption, extraction and mirror) and electrical transport losses.

The most obvious figure of merit obtained from the IV-IV measurement is the coupling quantum efficiency (CQE) of the system which we define as the ratio $\eta_{\mathrm{CQE}} = I_2/I_1$ where I_1 is the current injected through the DHJ LED and I_2 is the photocurrent generated in the lower diode when it is used as a photodetector under short circuit or moderate reverse bias conditions (Fig. 1). When the emission spectrum of the DHJ LED is known, the same measurement also allows estimating the power transfer efficiency of the system as $\eta = \eta_{\mathrm{CQE}}\hbar\omega/(qU_1)$, where $\hbar\omega$ is the average energy of the generated photons and U_1 is the voltage over the DHJ LED. In this formula, η can exceed unity when $qU_1 < \eta_{\mathrm{CQE}}\hbar\omega$. Observing this condition would imply net cooling of the DHJ LED.

Table II
THE MAIN GEOMETRICAL PARAMETERS OF THE MESAS AND THE CAPPING
LAYER DETERMINING THE ODR CONFIGURATION IN THE PROCESSED
DEVICES. MESA TYPES ARE IDENTIFIED BY RUNNING LOWER CASE
LETTERS.

Mesa type	Fill factor	Dot radius (um)	Mesa radius (um)	Number of dots / mesa
a	1	-	all	-
b	0.5	50.51	500	37
c	0.2	10	500	430
d	0.1	52.7	500	7
e	0.1	31.62	500	20
f	0.1	22.58	500	37
g	0.02	10.00	500	37
h	0.05	15.97	500	37
i	0.5	25.25	250	37
j	0.2	10	250	91
k	0.02	10	250	7
l	0.1	19.76	250	10
m	0.1	15.81	250	19
n	0.05	13.97	250	14
o	0.2	10	100	7
p	0.5	17.68	100	7
q	0.5	14.14	100	9
r	0.05	7	100	7
s	0.02	7	100	3
t	0.1	7.45	100	7
u	0.5	11.79	50	7
v	0.1	7.91	50	4
x	0.2	7	50	7
y	0.05	5.59	50	4

In addition to CQE, analyzing the IV-IV measurements in more detail can reveal information about the quality and the most important material and device parameters of the DHJ LEDs. In an ideal LED the recombination processes in the AL generally consist of three different classes of processes: the Shockley-Read-Hall (SRH), radiative and Auger recombination processes. The current density components generated by these processes ideally follow the so called ABC-model[12], with $J_{\mathrm{SRH}} = q\,d\,A\,n$, $J_{\mathrm{R}} = q\,d\,B\,n^2$ and $J_{\mathrm{A}} = q\,d\,C\,n^3$, where q is the elementary charge, d is the thickness of the LED AL, A, B and C are the SRH, radiative and Auger recombination coefficients, respectively and $n \sim \sqrt{n\,p} = n_{\mathrm{i}}\exp[q\,U/(2k_{\mathrm{B}}\,T)]$, where n and p are the electron and hole densities, n_{i} is the intrinsic carrier concentration, $U \leq U_1$ is the voltage over the ideal LED, k_{B} is the Boltzmann constant and T is the temperature. Writing the carrier density as $\sqrt{n\,p}$ is in many cases an oversimplification, but as seen in Section III it seems to be a very good approximation for our devices. The ideality factor

$$\gamma = \frac{q}{k\,T}\left[\frac{\mathrm{d}\ln J}{\mathrm{d}U}\right]^{-1} \qquad (1)$$

corresponding to each separate recombination model is therefore 2, 1 and 2/3 respectively.

To estimate the key device parameters we approximate the A and B parameters of our devices using the ABC model and the corresponding relations $A \sim J/[q\,d\,n_{\mathrm{i}}\exp(q\,U/2k_{\mathrm{B}}T)]$ and $B \sim J/[q\,d\,n_{\mathrm{i}}^2\exp(q\,U/k_{\mathrm{B}}T)]$. Another estimate for the SRH recombination coefficient A that is insensitive to possible differences between U and U_1, is obtained by using a relation

$A = J_{\mathrm{SRH}}\sqrt{B}/\sqrt{J_R q d}$ and a literature value for B. In addition we also use the characteristics of droop to estimate the internal quantum efficiency (IQE), photodiode capture efficiency and selected two values of the A, B and C parameters [13]. In the droop-fit method the photodiode capture efficiency (ratio of detected photons to bimolecular recombination events) is given as $x_{\mathrm{i}} = \eta_{\mathrm{m}}^2/(\eta_{\mathrm{m}} + 4D_2/\ln(10)^2)$ where η_{m} is the maximum of η_{QE} and D_2 is the second derivative of η_{m} with respect to $\lg(J)$. The IQE is then approximated as $\eta_{\mathrm{IQE}} \sim \eta_{\mathrm{m}}/x_{\mathrm{i}}$.

Another important loss mechanism arises from the mirror losses. Estimating the reflection coefficients of the metal contacts using only the measurement data is not very straightforward. Therefore, in addition to comparing the indicative experimental results obtained for different ODR fill factors, we also calculated the reflection coefficients for the contacts using the following well known relations.

The single-interface Fresnel reflection coefficients for the electric fields for s- and p-polarizations in a nonmagnetic structure are given by[14]

$$r_{\mathrm{s}} = \frac{n_1\cos\theta_1 - n_2\cos\theta_2}{n_1\cos\theta_1 + n_2\cos\theta_2}, \qquad (2)$$

$$r_{\mathrm{p}} = \frac{n_2\cos\theta_1 - n_1\cos\theta_2}{n_2\cos\theta_1 + n_1\cos\theta_2}, \qquad (3)$$

where

$$\theta_2 = \arcsin\left(\frac{n_1}{n_2}\sin\theta_1\right), \qquad (4)$$

n_1 and n_2 are the refractive indices of the two media around the interface, and θ_1 and θ_2 the incidence and refractive angles respectively.

Multiple interface reflection coefficients needed to calculate the reflection coefficients of the AlGaAs/GaAs/Ti/Au and AlGaAs/Si$_3$N$_4$/Ti/Au stacks are given in terms of the single interface reflection coefficients as a recursive relation

$$\mathcal{R}_{\sigma,m} = \frac{r_{\sigma,m} + \mathcal{R}_{\sigma,m+1}e^{2ik_{\mathrm{z},m+1}d_{m+1}}}{1 + r_{\sigma,m}\mathcal{R}_{\sigma,m+1}e^{2ik_{\mathrm{z},m+1}d_{m+1}}}, \qquad (5)$$

where d_m represent the layer thicknesses, $\sigma \in \{s,p\}$ the light polarization, $m \in \{1,2,...,N\}$ the interface number, $\mathcal{R}_{\sigma,N+1} = 0$ and the wave number in direction of propagation is $k_{\mathrm{z},m} = \sqrt{k_m^2 - (k_1\sin\theta_1)^2}$ with $k_m = \omega n_m/c$.

The direction averaged power reflection coefficients for layer 1 are then obtained as

$$R_1 = \sum_{\sigma=s,p}\int_0^{\pi/2}|\mathcal{R}_{\sigma,1}(\theta_1)|^2\sin\theta_1\cos\theta_1 d\theta_1 \qquad (6)$$

Using the parameters in Table III, the direction averaged power reflection coefficient for the Al$_{0.5}$Ga$_{0.5}$As/SiN/Ti/Au interface is $R_1 = 0.99$ and for the Al$_{0.5}$Ga$_{0.5}$As/GaAs/Ti/Au interface the reflection coefficient is $R_1 = 0.89$ for the wavelength $\lambda = 867$ nm.

III. RESULTS AND DISCUSSION

To gain the necessary insight and to demonstrate the basic operation of the intracavity systems we analyze the IV-characteristics of the DHJ LED and the corresponding photodiode of Fig. 1. Fig. 3a) shows the current densities of the DHJ LED and the photodiode on a linear scale as

Table III
MATERIAL PERMITTIVITIES AND REFRACTIVE INDICES USED IN THE
REFLECTANCE CALCULATIONS. THE METAL PERMITTIVITIES ARE
OBTAINED USING THE DRUDE MODEL WITH $\omega_p = 2.5168$ AND
$\omega_\tau = 0.04736$ [15] FOR TI AND $\omega_p = 8.89$ AND $\omega_\tau = 0.07088$ [16] FOR
AU.

Material	Permittivity	Refractive index
GaAs	13.310+0.826i	3.650+0.113i [17], [18]
$Al_{0.5}Ga_{0.5}As$	10.24	3.20 [19]
SiN	4.00	2.00 [20]
Ti	-2.094+0.102i	0.035+1.448i
Au	-37.552+1.911i	0.156+6.130i

functions of the bias voltage U_1 and a linear fit to the large current density region where the IV behaviour is dominated by the internal resistance. In Fig. 3b) the absolute values of the current densities are shown on a logarithmic scale along with ideal diode curves with ideality factors of 1 and 2 fitted to the purely exponential parts of the IV curves. The figures also show in gray dashed lines the voltage corresponding to the GaAs band gap (1.42 eV) and the voltage corresponding to 80 % of the gap which would allow cooling with $\eta_{QE} = 80$ %.
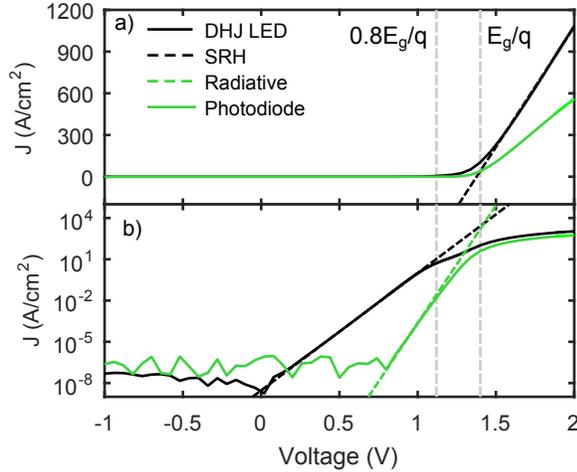

Figure 3. a) The IV curve for a DHJ LED and a photodiode on a linear scale and a line fitted to the large current density region of the LED, and b) the IV curves of the LED and photodiode as well as ideal diode fits with ideality factors of 1 and 2.

The fits clearly demonstrate that the operation of the DHJ LED is dominated by SRH-like recombination up to voltages of ~ 1 V and current densities of ~ 1 A/cm^2 while the current of the photodiode closely follows the bimolecular form. At voltages exceeding 1 V, however, the IV characteristics of the LED exhibit somewhat unconventional features. Instead of the transition to the bimolecular ($\gamma = 1$), Auger ($\gamma = 2/3$) or simple resistance dominated region most commonly observed in LEDs [21], Fig. 3b) shows a two step resistive saturation where the IV temporarily seems to recover from the resistive-like onset of saturation between U_1=1.1–1.4 V before finally becoming fully resistive. The conclusive reason for the two step onset of the resistive losses has not been established, but we suspect it is caused by the fast increase of the photodiode current density J_2 which allows a more significant fraction of

the current J_1 to flow through the photodiode. This results in a substantial reduction in the effective resistance of the lateral current spreading layer of the DHJ LED.

Considering the condition that $U \leq U_1$ in the ABC model of the previous section the expressions for A and B can be written as $A \geq J/[q\,d\,n_i \exp(qU_1/2k_BT)]$ and $B \geq J/[q\,d\,n_i^2 \exp(qU_1/k_BT)]$. For the data presented in Fig. 3 this results in $A \geq 4 \times 10^8$ s^{-1} and $B \geq 2 \times 10^{-10}$cm^{-3}s^{-1}. By using an exponential fit to the exponential parts of the LED and photodiode responses with conditions $J_{SRH} \sim J_1$ and $J_R \geq J_2$ we also recover a relation $A \leq J_1\sqrt{B}/(J_2qd)$. For the data in Fig. 3 this results in the SRH recombination coefficient $A \leq 7 \times 10^8$ s^{-1}. Combining these two results for A we therefore get 4×10^8 s$^{-1} \leq A \leq 7 \times 10^8$ s^{-1}. In addition to these methods, we estimated the IQE and photodiode efficiencies by using the droop fit method, which resulted in values $\eta_{IQE} \sim 68$ % and $\xi \sim 77$ %. Using the related equations 6 and 7 in Ref [13] along with the conventional literature value of $C \sim 10^{-30}$ cm^{6}s^{-1} for GaAs[22] gives $A \sim 9 \times 10^6$ s^{-1} and $B \sim 1 \times 10^{-10}$cm^{-3}s^{-1}, which slightly underestimates B compared to values reported in literature and underestimates A in comparison to the other fits. The variation in the values for different methods can be explained by their approximate nature and device heating, which is not considered in the estimations and is known to affect the droop-fit method. In any case we can conclude that SRH like recombination in the devices is significantly larger than in the best reported devices, which is also in qualitative agreement with the time resolved photoluminescence measurements we performed before any processing of the devices.

Figure 4 shows the CQE as a function of the DHJ LED current density for devices with 100 μm diameter mesas and a contact fill factor of 100 % for AL thicknesses of 300, 50 and 10 nm, corresponding to B1, B2 and B3, respectively. The CQE increases with increasing current up to current densities of $\sim$ 300–800 A/cm^2 and then starts to decrease showing a clear tendency of efficiency droop. A clear trend of a decreasing peak CQE with a decreasing AL thickness is also visible. This leads to several qualitative conclusions about the factors limiting the efficiency. First, it suggests that the current spreading in the shared n-type contact layer does not strongly affect the efficiency; If it did, the thin AL devices, where the total current is smaller, should perform better than the thick AL devices. Second, it also suggests that (bulk) nonradiative recombination in the AL is not the main factor causing the decrease in the CQE either as it would make the QE independent of the AL thickness. This leaves two primary explanations for the reduction: more pronounced non-isotropic emission from the thin AL leading to increased emission at oblique angles as well as the interface recombination at the GaAs/AlGaAs interfaces or recombination/leakage outside the AL.

Fig. 5 shows η_{QE} as a function of the DHJ LED current density J_1 for selected 100 μm diameter mesas on epistructure B1 with various contact fill factors in the p-contact. The device with the fill factor of 100 % exhibits the lowest QE value as expected, due to the largest reflection losses. The QE of the devices with fill factors of 50 % and 20 % are 52 % and
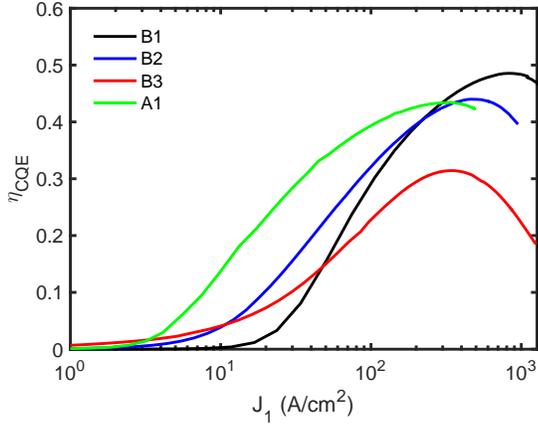
Figure 4. The CQE as a function of J_1 of DHJ LEDs with varying AL thickness (300 nm for B1, 50 nm for B2 and 10 nm for B3) and 100 μm mesas without ODR.

53 %, respectively. This is well in line with the reflectivity calculations, suggesting that the angle averaged reflectivity of the GaAs/metal mirror is 89 % while the reflectivity of the SiN/metal ODR is calculated to be 99 %. For the 100 % fill factor the optical loss is therefore estimated to be $\sim$ 5 % (only half of the emitted photons are emitted towards the contact) while for the 50 % and 20 % fill factor devices the losses would scale to $\sim$ 3 and 2 %, respectively. This suggests that while mirror losses are not negligible, they can be engineered to be sufficiently small to allow reaching the EL cooling regime.
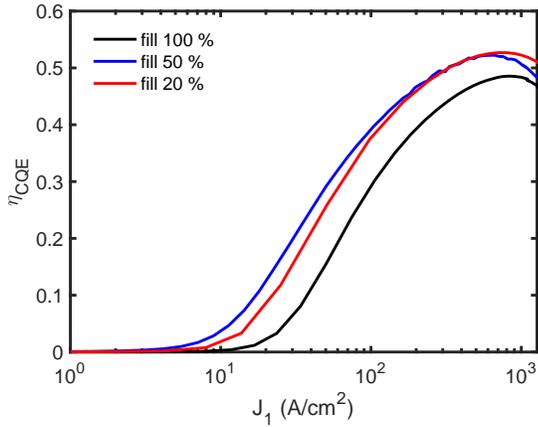

Figure 5. The CQE as a function of J_1 for devices with a varying p-contact metal fill factor. The two devices with the higher CQE have ODR mirrors embedded in the capping layers of the DHJ LED.

In order to estimate the fraction of losses resulting from light escaping the encapsulated semiconductor structure through the mesa side walls, IV-IV measurements were also carried out with selected devices submerged in a high refractive index medium, i.e. water (n_r=1.3) and transparent oil (n_r=1.5). Figure 6 shows the $\eta_{CQE}(J_1)$ the measurement results for two devices measured first in air followed by a measurement with the samples immersed in oil. While immersed in oil, the

CQE is lower for all devices compared to in-air measurements with an average decrease in the CQEs of approximately 1 %-unit near the peak CQE regions. Since the edge emission is expected to scale approximately in proportion to the square of the refractive index of the lower index media, this suggests that edge emission can only account for approximately 1 % of the losses even in the 100 μm diameter devices. The measurements done in water exhibit similar behaviour leading to the same conclusion.
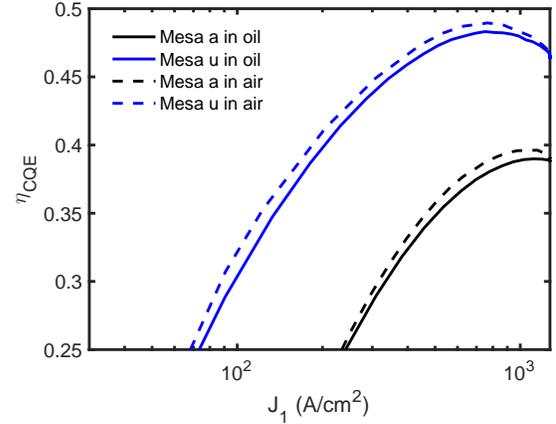

Figure 6. Comparison of $\eta_{CQE}(J_1)$ of DHJ LEDs in air and immersed in transparent oil. The immersion causes a slight decrease in the peak CQE for the devices.

To investigate the properties of the photodiode component alone, we also characterized its response to external light. The photodiodes were exposed by etching the epistructure from the top side to the common n-type layer (layer 8 in Table I), effectively removing the top LED structure. Electric metal contacts were then evaporated on the devices and the current through the devices was measured during a monochromatic low power optical excitation with tunable wavelength. Figure 7 shows the normalized EL spectrum of the edge emitted light of the DHJ LED and the QE (defined as the ratio of the photocurrent to the excitation photon number) of the corresponding photodiode as a function of wavelength for the photodiode of epistructure B1. The peak of the EL spectrum lies at approximately 867 nm which coincides roughly with the cut-off wavelength of the photodiode.

The maximum QE of the photodiode was found to be slightly below 90 % with an excitation power of 30 μW under short circuit conditions. The relatively low value can be partly explained by the low excitation power and relatively large ($\sim$ 1 cm^2) area of the device as well as potential calibration deficiencies of the measurement, as we used a simple hand-held power meter for estimating the pump power.

Overall our results suggest that the losses in the energy transfer in our first intracavity setup are mainly formed of mirror losses ($\sim$ 1-5 %), edge emission losses ($\sim$ 1 %) as well as material related losses and potential free carrier absorption losses. Based on the present results, the order of magnitude of the two latter loss mechanisms is still partly unknown, but based on the estimated values of the SRH coefficient A, we presently expect that most of the 30–40 % overall losses
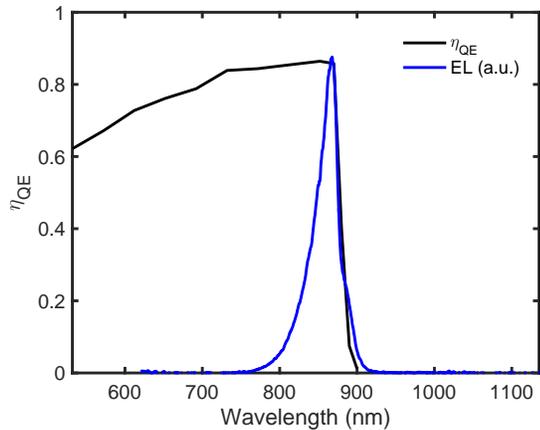
Figure 7. The EL and QE spectra of the DHJ LED and the corresponding photodiode structure, respectively.

are due to partly unoptimized materials. Additionally, because several reports suggest that the material quality can be substantially improved allowing notable decrease in nonradiative recombination, we expect that the losses can be relatively quickly reduced to below the level of 10–20 %, which we expect to be sufficient to reach the large current density EL cooling regime.

The key challenges in further development of the devices involve developing and adapting suitable measurement and modeling techniques that allow for understanding and optimizing the internal losses in the studied structures and scaling up their surface area. Unlike in our previous studies of InP based devices [23], the studied GaAs based devices appear to allow much easier scaling of the device size as only few of the fabricated samples have shown pronounced leakage we frequently observed in the InP devices. At present we cannot fully determine the role of leakage currents through the DHJ LED in the device operation. In principle the leakage current component might enable transistor-like operation, and will require additional investigations, but based on general expectations and in particular on observing the droop-like efficiency reduction at high currents strongly suggests that possible leakage current issues in the structures are negligible.

IV. CONCLUSIONS

We have fabricated, characterized and analyzed the performance of an intracavity light emitter setup, where a light absorbing element is located in the same high refractive index host crystal as the emitter. This layout fully overcomes the light extraction challenges of conventional light emitters where the high refractive index contrast leads to strong optical confinement. We estimated the contributions of key loss mechanisms to the system performance. Results show a current-to-current conversion efficiency that depends quite strongly on the design parameters of the structures and reaches maximum values below 60 % with our present devices. In contrast to laser cooling experiments where even quantum efficiencies exceeding 99 % are not sufficient [11], we expect that for EL cooling using the intracavity configuration a QE of the

order of 80-90 % would allow demonstrating the cooling. Since our results also suggest that after further optimization none of the observed losses should be too high to reach over 90 % quantum efficiencies, we expect that the intracavity configuration provides an excellent platform for further studies and optimization of EL cooling of III-V semiconductors.

REFERENCES

[1] Shuji Nakamura and M. R. Krames. History of Gallium Nitride-Based Light-Emitting Diodes for Illumination. *Proceedings of the IEEE*, 101(10):2211–2220, October 2013.

[2] Mircea Guina, Antti Härkönen, Ville-Markus Korpijärvi, Tomi Leinonen, and Soile Suomalainen. Semiconductor Disk Lasers: Recent Advances in Generation of Yellow-Orange and Mid-IR Radiation. *Advances in Optical Technologies*, 2012:1–19, 2012.

[3] Mansoor Sheik-Bahae and Richard I. Epstein. Optical refrigeration. *Nature Photonics*, 1(12):693–699, December 2007.

[4] Jun Zhang, Dehui Li, Renjie Chen, and Qihua Xiong. Laser cooling of a semiconductor by 40 Kelvin. *Nature*, 493(7433):504–508, January 2013.

[5] Jin Xue, Yuji Zhao, Sang-Ho Oh, William F. Herrington, James S. Speck, Steven P. DenBaars, Shuji Nakamura, and Rajeev J. Ram. Thermally enhanced blue light-emitting diode. *Applied Physics Letters*, 107(12):121109, September 2015.

[6] Jani Oksanen and Jukka Tulkki. Thermophotonics: LEDs feed on waste heat. *Nature Photonics*, 9(12):782–784, November 2015.

[7] Duanni Huang, Parthiban Santhanam, and Rajeev J. Ram. Low-power communication with a photonic heat pump. *Optics Express*, 22(S7):A1650, December 2014.

[8] Parthiban Santhanam, Dodd Gray, and Rajeev Ram. Thermoelectrically Pumped Light-Emitting Diodes Operating above Unity Efficiency. *Physical Review Letters*, 108(9), February 2012.

[9] Parthiban Santhanam, Duanni Huang, Rajeev J. Ram, Maxim A. Remennyi, and Boris A. Matveev. Room temperature thermo-electric pumping in mid-infrared light-emitting diodes. *Applied Physics Letters*, 103(18):183513, 2013.

[10] Ryan P. Martin, Josef Velten, Andreas Stintz, Kevin J. Malloy, Richard I. Epstein, Mansoor Sheik-Bahae, Michael P. Hasselbeck, Babak Imangholi, S. T. P. Boyd, and Todd M. Bauer. Nanogap experiments for laser cooling: a progress report. pages 64610H–64610H–4, February 2007.

[11] Daniel A. Bender, Jeffrey G. Cederberg, Chengao Wang, and Mansoor Sheik-Bahae. Development of high quantum efficiency GaAs/GaInP double heterostructures for laser cooling. *Applied Physics Letters*, 102(25):252102, 2013.

[12] Marius Grundmann. *The Physics of Semiconductors: An Introduction Including Nanophysics and Applications*. Graduate Texts in Physics. Springer International Publishing, 2016.

[13] Pyry Kivisaari, Lauri Riuttanen, Jani Oksanen, Sami Suihkonen, Muhammad Ali, Harri Lipsanen, and Jukka Tulkki. Electrical measurement of internal quantum efficiency and extraction efficiency of III-N light-emitting diodes. *Applied Physics Letters*, 101(2):021113, 2012.

[14] Eugene Hecht. *Optics*. Pearson education. Addison-Wesley, 2002.

[15] M. A. Ordal, L. L. Long, R. J. Bell, S. E. Bell, R. R. Bell, R. W. Alexander, and C. A. Ward. Optical properties of the metals Al, Co, Cu, Au, Fe, Pb, Ni, Pd, Pt, Ag, Ti, and W in the infrared and far infrared. *Appl. Opt.*, 22:1099–1119, 1983.

[16] Ellen J. Zeman and George C. Schatz. An accurate electromagnetic theory study of surface enhancement factors for silver, gold, copper, lithium, sodium, aluminum, gallium, indium, zinc, and cadmium. *J. Phys. Chem.*, 91:634–643, 1987.

[17] J. S. Blakemore. Semiconducting and other major properties of gallium arsenide. *J. Appl. Phys.*, 53:R123–R181, 1982.

[18] M. D. Sturge. Optical absorption of gallium arsenide between 0.6 and 2.75 eV. *Phys. Rev.*, 127:768–773, Aug 1962.

[19] David W. Jenkins. Optical constants of $Al_xGa_{1-x}As$. *J. Appl. Phys.*, 68(4):1848–1853, 1990.

[20] Herbert R. Philipp. Optical properties of silicon nitride. *J. Electrochem. Soc.*, 120:295–300, 1973.

[21] E. Fred Schubert. *Light-emitting diodes*. Cambridge University Press, Cambridge ; New York, 2nd ed edition, 2006.

[22] U. Strauss, W. W. Rühle, and K. Köhler. Auger recombination in intrinsic gaas. *Applied Physics Letters*, 62(1), 1993.

[23] Anders Olsson, Abuduwayiti Aierken, Henri Jussila, Jan Bauer, Jani Oksanen, Otwin Breitenstein, Harri Lipsanen, and Jukka Tulkki. Yield and leakage currents of large area lattice matched InP/InGaAs heterostructures. *Journal of Applied Physics*, 116(8):083105, August 2014.